Since January 2020 Elsevier has created a COVID-19 resource centre with free information in English and Mandarin on the novel coronavirus COVID-19. The COVID-19 resource centre is hosted on Elsevier Connect, the company's public news and information website.

Journal of Infection 83 (2021) 197–206

Contents lists available at ScienceDirect

Journal of Infection

journal homepage: www.elsevier.com/locate/jinf

Structural dynamics of SARS-CoV-2 variants: A health monitoring strategy for anticipating Covid-19 outbreaks

Jacques Fantini[a,b,*], Nouara Yahi[a,b], Fodil Azzaz[a,b], Henri Chahinian[a,b]

[a] INSERM UMR_S 1072, 13015 Marseille, France
[b] Aix-Marseille Université, 13015 Marseille, France

ARTICLE INFO

Article history:
Accepted 1 June 2021
Available online 3 June 2021

Keywords:
SARS-CoV-2
Coronavirus
Lipid raft
Ganglioside
Electrostatic surface potential
ACE-2
receptor
Virus-host interactions

SUMMARY

Objectives: the Covid-19 pandemic has been marked by sudden outbreaks of SARS-CoV-2 variants harboring mutations in both the N-terminal (NTD) and receptor binding (RBD) domains of the spike protein. The goal of this study was to predict the transmissibility of SARS-CoV-2 variants from genomic sequence data.

Methods: we used a target-based molecular modeling strategy combined with surface potential analysis of the NTD and RBD.

Results: we observed that both domains act synergistically to ensure optimal virus adhesion, which explains why most variants exhibit concomitant mutations in the RBD and in the NTD. Some mutation patterns affect the affinity of the spike protein for ACE-2. However, other patterns increase the electropositive surface of the spike, with determinant effects on the kinetics of virus adhesion to lipid raft gangliosides. Based on this new view of the structural dynamics of SARS-CoV-2 variants, we defined an index of transmissibility (T-index) calculated from kinetic and affinity parameters of coronavirus binding to host cells. The T-index is characteristic of each variant and predictive of its dissemination in animal and human populations.

Conclusions: the T-index can be used as a health monitoring strategy to anticipate future Covid-19 outbreaks due to the emergence of variants of concern.

Introduction

SARS-CoV-2 variants with mutations in the spike protein are suspected to cause Covid-19 outbreaks in various countries worldwide.[1–4] Such variants of concern (VOC) pose a serious problem of public health since they may combine an increased transmissibility and resistance to neutralizing antibodies. It is thus of critical importance to assess the potential dangerousness of variants as soon as they are detected by genomic sequence analysis. The spike protein, which initiates the first contact between the virus and the host cell surface, plays a key role in the control of SARS-CoV-2 infectivity.[5] It is organized as a trimer in which each subunit displays two domains distant from the virus envelope (Fig. 1). The first domain referred to as the receptor binding domain (RBD), lies in the central area of the trimer and is devoted to the recognition of a specific protein receptor on the host cell membrane, essentially ACE-2.[6] The other domain, referred to as the N-terminal domain (NTD), is rejected on the side, defining a typical tripod topology of the trimer.[5] This topology of the three NTDs may considerably improve the docking of the spike to gangliosides-rich domains (lipid rafts) which are the privileged sites of virus landing (Fig. 1A), and the subsequent delivery of the spike-raft complex to ACE-2 (Fig. 1B) by a "surf-like" process,[5,7] as shown for other enveloped viruses.[8,9]

Gangliosides are negatively charged at physiological pH.[10,11] Thus, the electrical surface potential of a lipid raft is negative (acidic) so that the microbial adhesins and toxins are generally basic (positively charged).[12] Under these conditions, the initial association of microbial proteins with lipid rafts is essentially mediated by an electrostatic interaction,[13] which has to be considered for predicting virus transmissibility.

In this study, we developed a global *in silico* analysis of virus binding to host cells and determined the impact of both RBD and NTD mutations in this process. For each virus isolate (Table 1), we determined: i) the surface potential of the NTD and of the RBD, ii) the overall avidity of the NTD for lipid raft gangliosides, and iii) the affinity of the RBD for ACE-2. All these characteristics were

* Corresponding author at: INSERM UMR_S 1072, 13015 Marseille, France.
E-mail address: jacques.fantini@univ-amu.fr (J. Fantini).

https://doi.org/10.1016/j.jinf.2021.06.001
0163-4453/

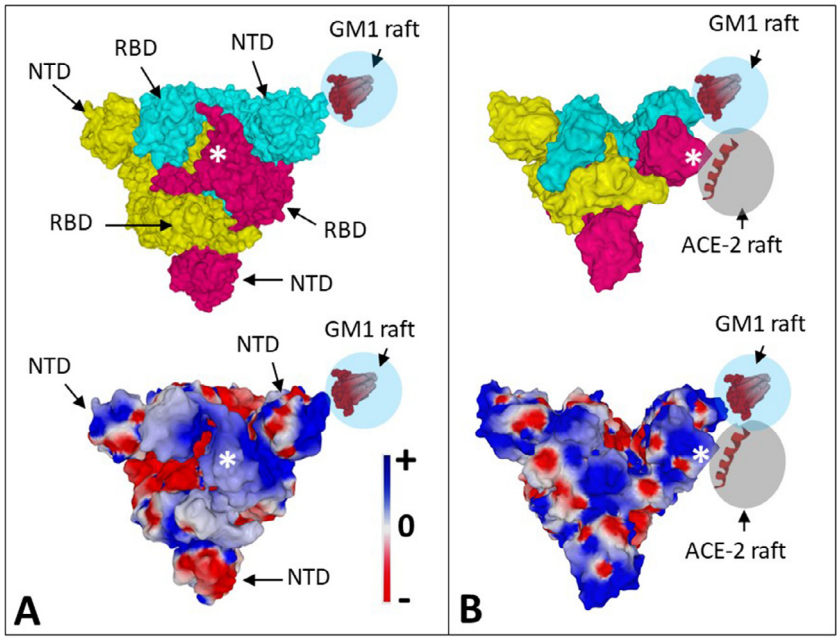

Fig. 1. Topology of SARS-CoV-2 spike trimer in the closed and open states. A. The closed conformation of SARS-CoV-2 spike trimer is retrieved from pdb file 7VSB. The trimer is viewed from the top, facing the host cell membrane (upper panel). Subunits A, B, and C of the pdb file are colored in cyan, yellow and purple, respectively. The white asterisk on the RBD of chain C indicates the center of the ACE-2 binding motif around residue Y-489. The electrostatic surface potential of the spike is represented in the lower panel. The NTD of the A chain is bound to a GM1 lipid raft. **B.** The open conformation of SARS-CoV-2 spike trimer is retrieved from pdb file 7DK3. The RBD of the C chain has moved in the direction of the NTD of chain A so that the lining residues that bind to ACE-2 are now rejected at the periphery of the spike (upper panel, white asterisk). Since ACE-2 is a lipid raft associated protein, an ACE-2 raft may thus bind and coalesce with the GM1 raft already bound to the NTD of chain A, increasing the probability of a functional contact between the spike and the ACE-2 receptor. Note that at this stage, all three NTDs display an electropositive surface potential consistent with the recruitment of several lipid rafts around the viral spike (lower panel). During this lipid raft controlled process, the closed state moves from an ACE-2 inaccessible to an ACE-2 accessible topology (open state). The color scale for the electrostatic surface potential (negative in red, positive in blue, neutral in white) is indicated. (For interpretation of the references to colour in this figure legend, the reader is referred to the web version of this article.).

Table 1
Mutations in the NTD and in the RBD of SARS-CoV-2 variants.

Virus strain	NTD	RBD
UK B.1.1.7	Deletion H69-V70 Deletion Y144	N501Y
Brazil B.1.1.248	L18F T20N P26S D138Y R190S	K417T E484K N501Y
South Africa B.1.351	L18F D80A D215G Deletion L242-A243-L244	K417N E484K N501Y
India B.1.617	G142D E154K	L452R E484Q

translated and summarized in a unique value, the T-index (transmissibility index) through a specially designed multiple modeling method. We propose to use the T-index as a health monitoring strategy for anticipating the emergence and development of SARS-CoV-2 variants that may cause Covid-19 outbreaks.

Methods

Molecular modeling studies were performed using Hyperchem (http://www.hypercubeusa.com), Deep View/Swiss-Pdb viewer (https://spdbv.vital-it.ch) and Molegro Molecular viewer (http://molexus.io/molegro-molecular-viewer) as described previously[14,15]. The initial coordinates of ganglioside GM1 were obtained from CHARMM-GUI Glycolipid Modeler[16] (http://www.charmmgui.org/?doc=input/glycolipid) which uses the internal coordinate information of common glycosidic torsion angle values and performs Langevin dynamics with a cylindrical restraint potential to keep the whole GM1 molecule cylindrical, especially the membrane-embedded ceramide part. The electrostatic potential measured and illustrated by Molegro Molecular viewer is the sum of the Coulomb potentials for each atom of the considered molecule, with a distance-dependent dielectric constant. Color intensities of the electrostatic surface potential were quantified with the ImageJ software.

Results

RBD-ACE-2 complex

The coordinates of the ACE-2 RBD complex were obtained from the pdb file 6M0J (B.1 Wuhan strain).[17] The model was submitted to 6 successive rounds of energy minimization to remove any steric clash and optimize the contacts between ACE-2 and the RBD. This refined model is shown in Fig. 2. The whole energy of interaction is estimated to -343 kJ/mol^{-1} after minimization, compared with -229 kJ/mol^{-1} in the non-minimized pdb file. Key amino acid residues involved in the complex are located in the 403–505 segment of the RBD and regions 19–53 and 81–84 of ACE-2 (Fig. 2A). The molecular forces that stabilize the complex consist in a sophisticated combination of van der Waals (Fig. 2B), electrostatic (Fig. 2C) and hydrogen bonding (Fig. 2D) that are regularly distributed over the contact zone between ACE-2 and the RBD surfaces (Fig. 2A). The side chains of apolar amino acid residues that are not buried in these proteins establish typical hydrophobic patches which exclude water molecules through an entropic driven mechanism. Such clusters are illustrated by the contacts between Y489 on the RBD and T27 on ACE-2, and Q498 on the RBD and L45 on ACE-2 (Fig. 2B). Of primary interest is a double and symmetric electrostatic bridge involving: i) K417 on the RBD and D30 on ACE-2, and ii) E484 on the RBD and K31 on ACE-2. This electrostatic bridge clamps the central zone of the complex, which limits the possibilities of conformational adjustments during the binding process. For this reason, it represents a hot mutational spot in

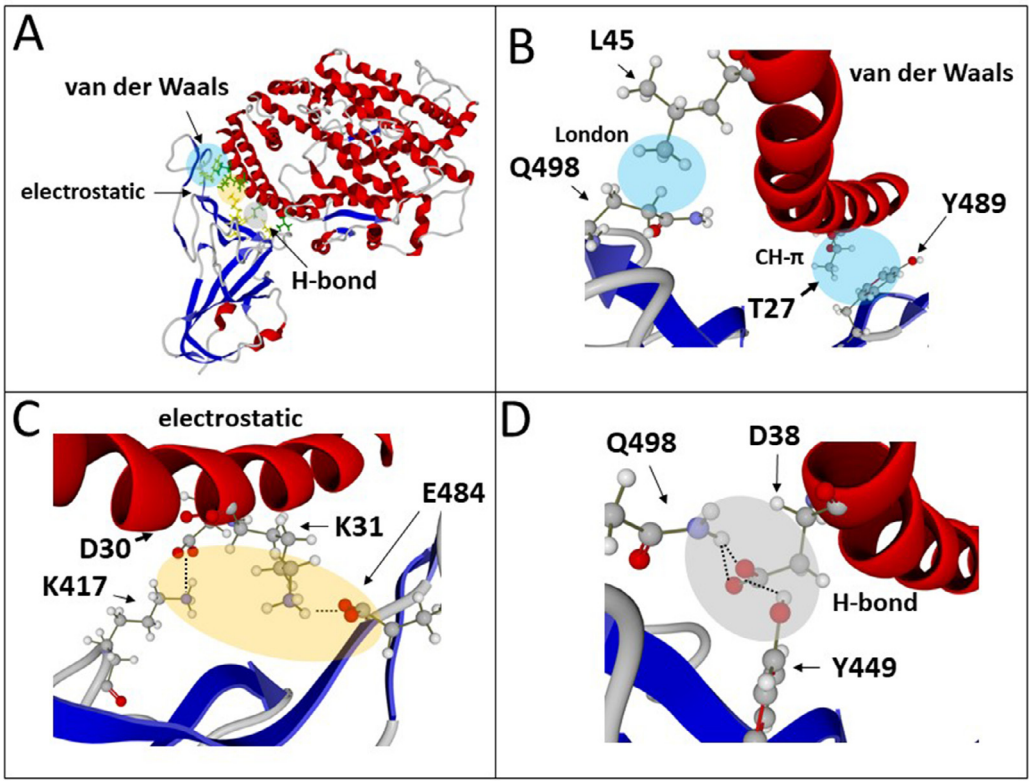

Fig. 2. Molecular mechanisms of RBD binding to ACE-2. A. Overall view of the RBD-ACE-2 complex showing the three main forces of stabilization: van der Waals, electrostatic and hydrogen bonding. **B.** Focus on van der Waals forces illustrated by Y489 and Q498 from the RBD interacting with T27 and L45 from ACE-2, respectively through London forces and CH-π stacking. **C.** Electrostatic interactions involving residues D30 and K31 from ACE-2 and K417 and E-484 from the RBD. **D.** A network of hydrogen bonds linking residues D-38 from ACE-2, and Y449 and Q498 from the RBD. (For interpretation of the references to color in this figure, the reader is referred to the web version of this article.)

SARS-CoV-2 variants. The third type of stabilization is provided by hydrogen bonds as illustrated with the H-bond network involving Y449 and Q498 on the RBD and D38 on ACE-2 (Fig. 2D). It is important to note that this detailed analysis describes the final state of the RBD-ACE-2 complex, so that it does not give any information on the binding kinetics. In other words, this type of analysis may allow comparing the affinity of various SARS-CoV-2 variants for ACE-2, which is a valuable yet an incomplete information. Indeed, variants displaying a similar affinity for ACE-2 may greatly differ in their kinetics of association with the receptor, which will obviously give to such "fast" variants a key advantage over others. For this reason, we decided to add a kinetic parameter to the classic affinity study of ACE-2-RBD complexes.

The electrostatic surface potential gives interesting clues for the comprehension of the kinetics of formation of the RBD-ACE-2 complex (Fig. 3A). Indeed, the surface potential of ACE-2 (Figs. 3B-C) is globally negative (red spots) yet with three little positive areas (blue spots). The surface potential of the RBD is chiefly electropositive (Figs. 3B-C) and it shows several complementary areas with respect to ACE-2 (Fig. 3B**, solid arrows**) as well as some repulsive zones (Fig. 3B**, dashed arrows**). Thus, mutations in the RBD that increase the electrostatic complementarity (or decrease charge repulsion) between the RBD and ACE-2 will speed up the binding process. As ACE-2 is globally negative, it is expected that such mutations increase the number of positive charges on the RBD surface.

NTD-raft complex

The atomic coordinates used for the NTD were obtained from pdb files 7DK3[18] and7L2C[19]. Most pdb files of the SARS-CoV-2 spike protein lack the 70–76 loop. For this reason, we created a new 3D structure file for the NTD by rebuilding this missing information with Hyperchem. The corrected 3D structure of the NTD was then submitted to 6 successive rounds of energy minimization as described for the RBD. The resulting minimized file was used as our source NTD file. As previously reported[20,21] the flat surface of the NTD is especially well fitted to interact with a lipid raft. Extending our previous modeling studies,[20,21] we simulated the landing of the NTD on a lipid raft surface containing six GM1 gangliosides. After energy minimization, a stable NTD-raft complex was obtained (Fig. 4A) in which all 6 GM1 molecules were bound to the NTD, occupying most of the available surface. The energy of interaction of this NTD-raft complex is estimated to -397 kJ.mol^{-1}, a value close to the one of the RBD-ACE-2 complex (-343 kJ.mol^{-1}). The surface potential of the raft is shown in Figs. 4B-C. It is homogenously electronegative, consistent with the presence of one sialic acid per GM1 ganglioside. As expected, the surface of the NDT displays large electropositive areas that provide a complementary surface for the raft. Nevertheless, one should also note that the presence of two electronegative spots, one central (amino acid residues 154–156) and the other one peripheral, on the left side of the domain (Fig. 4C). These electronegative areas may slow down the initial attraction of the NTD to lipid rafts and are thus susceptible to be affected in SARS-CoV-2 variants.

SARS-CoV-2 variants

From the combined analysis of the NTD and the RBD bound to their respective targets, one can conclude that both domains act in synergy to ensure a functional interaction of the spike with lipid rafts, and this step will be followed by ACE-2 binding. In this pro-

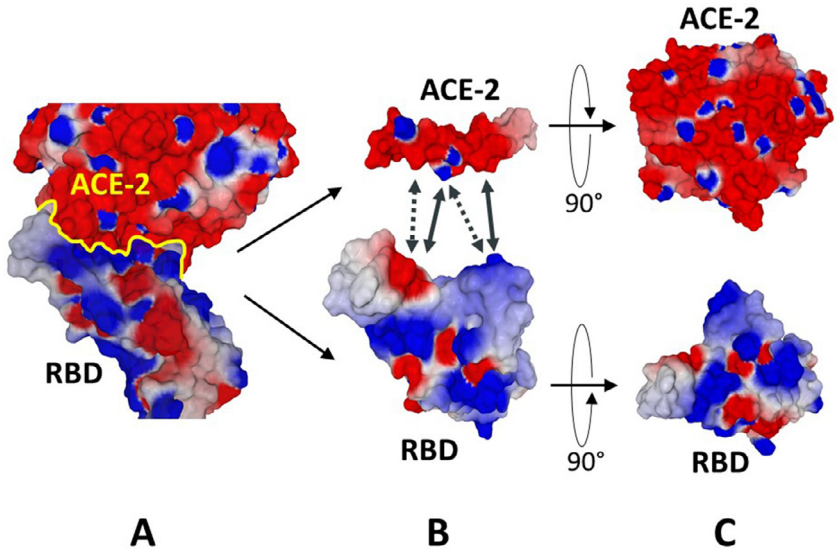

Fig. 3. ACE-2 and RBD electrostatic surface potential. A. RBD-ACE-2 complex. The yellow line shows the limit between the RBD and ACE-2 in the complex. **B.** Separate views of ACE-2 and of the RBD. Electrostatic attraction is represented by solid arrows, whereas electrostatic repulsion is indicated by dashed arrows. **C.** Bottom view of ACE-2 and top view of the RBD after 90° rotation. The electrostatic surface potential is represented in three colors: blue, electropositive, red, electronegative, white, neutral. (For interpretation of the references to colour in this figure legend, the reader is referred to the web version of this article.)

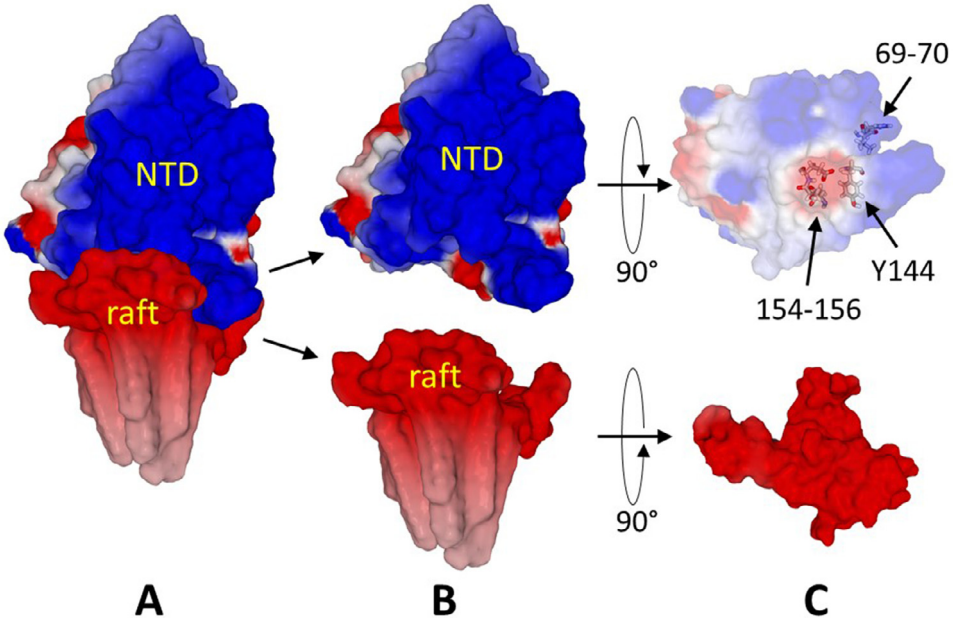

Fig. 4. Electrostatic surface potential of the NTD and a GM1 lipid raft. A. NTD-GM1 lipid raft complex. **B.** Separate views of the NTD and of the GM1 raft. **C.** A rotation of 90° of the NTD shows that its flat surface in contact with the raft has several electropositive regions around a central negative area corresponding to amino acid residues 154–156. The position 69–70 and 144 are indicated because these three amino acid residues are deleted in the UK variant of SARS-CoV-2. The GM1 lipid raft displays a homogenous electronegative surface.

cess, the electrical surface potential of the NTD and the RBD play a critical role in the attraction of the spike to lipid rafts. The more these domains are basic, the faster virus binding occurs.

SARS-CoV-2 variants (Table 1) were studied on the basis of the source files shown in Figs. 2–4. Mutations (either single points or deletions) were introduced in the spike protein, and then minimized before docking. All simulations led to a stable complex between any mutated RBDs and ACE-2.

The UK variant B.1.1.7[2] has one mutation in the RBD (N501Y) and two deletions in the NTD (del69–70 and del144). The impact of mutation N501Y for ACE-2 recognition is illustrated in Fig. 5. The aromatic side chain of tyrosine-501 clearly improves the interaction with ACE-2 by reinforcing the binding of lysine-353 and tyrosine-41 of ACE-2 (Fig. 5**C**). This stabilization involves the creation of a network of hydrogen bonds and the formation of a $\pi-\pi$ stacking interaction between the aromatic rings of tyrosine-501 (RBD) and tyrosine-41 (ACE-2) (Fig. 5**D**). Under these conditions, the energy of interaction concerning the 501 residue of the RBD reaches -27.2 kJ.mol^{-1} compared with -17.7 kJ.mol^{-1} for the Wuhan B.1 strain, i.e. a $\Delta G_{mut}/\Delta G_{wt}$ ratio of 1.53 (1.45 for the whole RBD-ACE-2 complex) (Table 2).

The analysis of the electrostatic surface potential of the UK B.1.1.7 RBD variant revealed two spots, one with decreased electronegativity, the other with increased electropositivity (Fig. 5**B**). Both changes concurred to confer a kinetic advantage of the RBD of this variant compared with the Wuhan B.1 isolate. A similar study

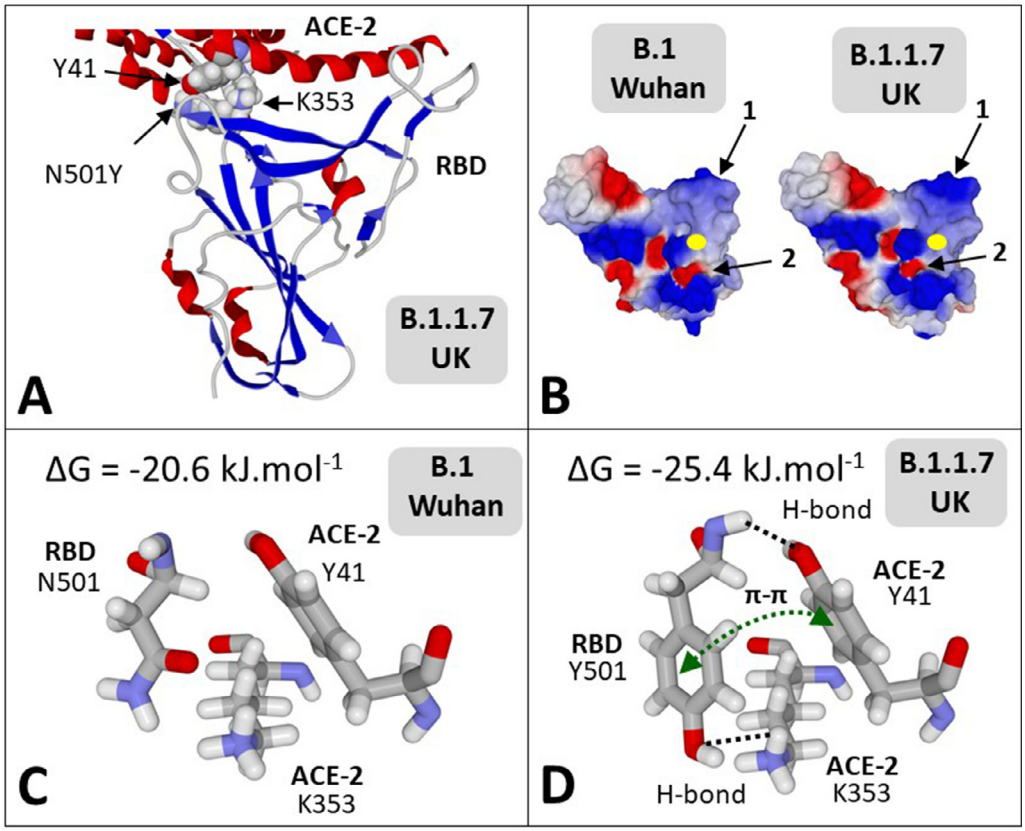

Fig. 5. Impact of the N501Y mutation (UK variant) of ACE-2 recognition. A. Overall view of the molecular complex between ACE-2 and the mutant RBD with the N501Y mutation. The mutant tyrosine-501 residue is in close contact with tyrosine-41 and lysine-353 of ACE-2. **B.** Electrostatic surface potential of the Wuhan (wt) and UK variant RBD displaying the N501Y mutation. The yellow disk indicates position 501 in both wt and mutant spike proteins. **C.** Interactions of asparagine-501 with ACE-2 residues 41 and 353. Although the three residues lie in the same area, they interact chiefly by van der Waals forces (energy of interaction −20.6 kJ. mol^{-1}). **D.** Network of hydrogen bonds and CH-π stacking involving the mutant residue tyrosine-501 of the UK variant (energy of interaction −25.4 kJ. mol^{-1}). (For interpretation of the references to colour in this figure legend, the reader is referred to the web version of this article.)

applied to the NTD also revealed a better electrostatic fit of the variant vs. Wuhan B.1 NTD (Fig. 6). The central acidic spot of the Wuhan B.1 NTD was split in two parts in the UK B.1.1.7 variant. The compaction induced by the deletions resulted in the formation of a large and continuous electropositive zone on the right side of the UK B.1.1.7 variant NTD (zones 2 and 3, Fig. 6). The histograms of red/blue intensities of the NTD surface confirmed that the UK B.1.1.7 variant was globally more electropositive and less electronegative than the Wuhan B.1 isolate. Taken together, the characteristics of the electrostatic surface potential of the UK B.1.1.7 variant in both the NTD and the RBD converged to confer a kinetic advantage of this virus compared to the Wuhan B.1 strain for the initial attraction to lipid raft gangliosides.

The Brazil variant B.1.1.248[1] has three mutations in the RBD: K417T, E484K and N501Y (Fig. 7**A**). The N501Y plays the same role as in the UK variant, with a stabilization of one side of the RBD-ACE-2 complex through locking residues K353 and Y41 ($\Delta G_{mut}/\Delta G_{wt}$ = 1.41). The case of the E484K mutation is more complex. In the non-minimized pdb file (Wuhan B.1 strain), glutamate-484 has very little interaction with ACE-2 (−1.4 kJ.mol^{-1}). However, after several rounds of energy minimization, the negative charge of this acidic residue could form an electrostatic bridge with the cationic charge of lysine-31 of ACE-2. The energy of interaction of this bond was estimated to −10.5 kJ.mol^{-1}. When glutamate-484 was substituted with lysine (E484K mutation), the electrostatic bridge was no longer possible because of the charge repulsion of lysine-484 and lysine-31 of ACE-2. Instead, the side chain of lysine-484 was rejected on the side, establishing stabilizing interactions with the methylene groups of lysine-31 (van der Waals) and tyrosine-83 (hydrogen bond) (Fig. 7**B**). In this configuration, the cationic NH_3^+ groups of lysine-484 and lysine-31 are oriented in opposite directions, avoiding any electrostatic repulsion. The energy of interaction between lysine-484 and ACE-2 reached −17.4 kJ.mol^{-1} ($\Delta G_{mut}/\Delta G_{wt}$ = 1.65). In the same time, the K417T mutation abrogated the contact between this residue and the ACE-2 receptor. Overall, these three mutations had compensatory effects on ACE-2 binding, so that the affinity of the Brazil variant spike for ACE-2 was globally not affected by this particular pattern of mutations ($\Delta G_{mut}/\Delta G_{wt}$ ratio of 1.02) (Table 2).

Then we analyzed the electrostatic surface potential of the RBD to assess the impact of mutations K417T, E484K and N501Y altogether (Figs. 7**C,D**). As expected, mutation K417T induced an inversion of the surface potential, from positive to negative. Mutation E484K resulted in a symmetric inversion, from negative to positive. Finally, mutation N501Y, in this mutational context, slightly increased the positive potential of the central area of the RBD. Thus, the mutated RBD of the Brazil B.1.1.248 variant has a stronger positive surface, consistent with a favorable kinetic effect of this variant for the recruitment of lipid rafts associated with ACE-2. Similar results were obtained after analyzing the surface potential of the NTD. The Brazil B.1.1.248 variant has 5 mutations in this domain: L18F, T20N, P26S, D138Y and R190S. Taken together, these mutations induced a dramatic rearrangement of the surface potential (Fig. 8). We identified 5 zones of reinforcement of the positive potential and/or decrease of negative potential. Overall, the mutated NTD of the Brazil B.1.1.248 variant has a far more electropositive

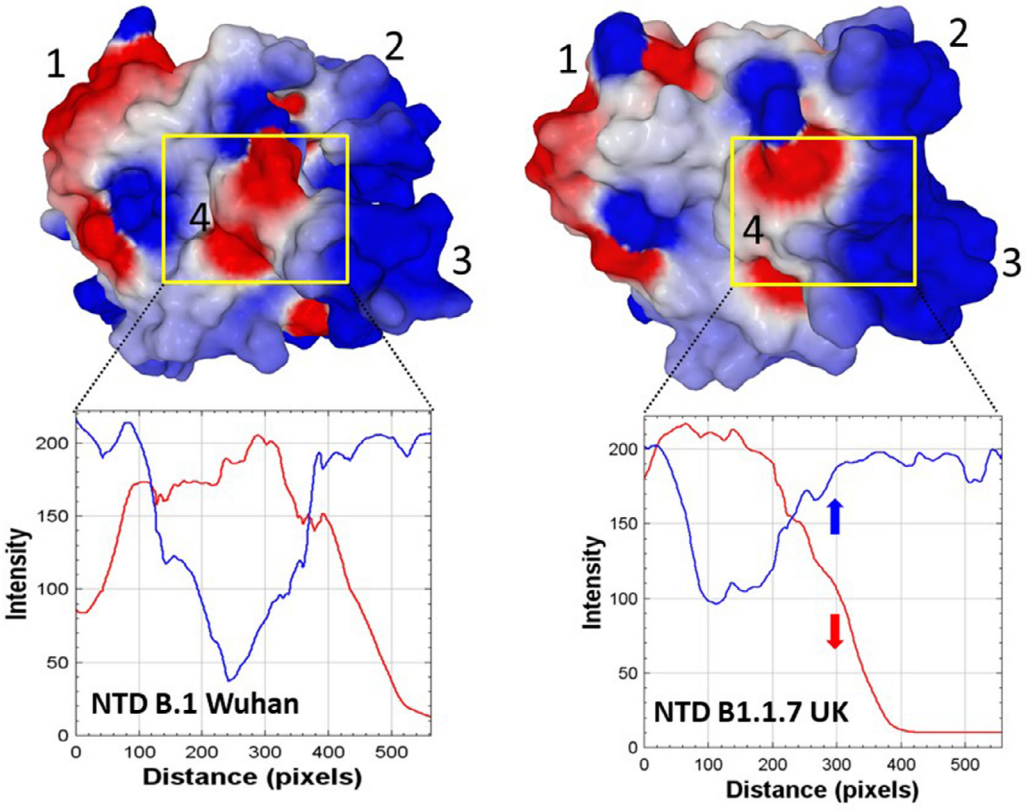

Fig. 6. Impact of deletions 69–70 and 144 (B.1.1.7 UK variant) on the surface potential of the NTD. The electrostatic surface potential of the B.1.1.7 variant NTD shows important electronic redistribution compared with the Wuhan B.1 NTD. The relative intensity of blue and red colors in the central region of the NTD (yellow frame) is indicated in the histograms. Changes in electrostatic potential affect four distinct zones numbered from 1 to 4. The deletions located in zones 2 and 3 increase the surface potential of the NTD. (For interpretation of the references to colour in this figure legend, the reader is referred to the web version of this article.)

surface than the Wuhan B.1 isolate, suggesting a decisive kinetic advantage for the initial interaction of the spike trimer with lipid rafts. As for the UK B.1.1.7 variant, it appears that both the RBD and the NTD surfaces evolved concomitantly toward a more positive, lipid-raft improved electrostatic surface.

This tendency to evolve toward a more positive surface of interaction is confirmed by an analysis of two other variants that are currently circulating in South Africa (B.1.351)[3] and India (B.1.617).[4] As shown in Fig. 9, both the NTD and the RBD of these variants display less electronegative spots and larger electropositive areas compared to the initial Wuhan B.1 strain. In the case of the Indian B.1.617, the difference in surface potential is likely to confer a selective advantage for the interaction with raft-associated receptors (gangliosides and ACE-2). The analysis of the affinity of those variants for gangliosides and ACE-2 did not reveal anything special as it fell in the range of affinity gain calculated for the other strains (Table 2). However, the combined analysis of affinity and kinetic parameters were summarized in 4 values for each virus that allowed us to define a transmissibility index (T-index). Given that the 4 parameters are totally independent, the T-index is calculated as the mathematical product of these 4 values (Table 2). T-index takes into account the avidity of the NTD for lipid raft gangliosides ($\Delta G_{mut}/\Delta G_{wt\ [NTD\text{-}ganglioside]}$), the affinity of the RBD for ACE-2 ($\Delta G_{mut}/\Delta G_{wt\ [RBD\text{-}ACE\text{-}2]}$), and a global estimation of the electrostatic surface potential of both the NTD and the RBD (kinetic parameter). Values of T-index ranged from 2.16 for the Wuhan B.1 strain to 10.67 for the India B.1.617 variant (ca. 500% increase of transmissibility). The T-index can be used as a straightforward scale for the classification of variants, and the identification of variants of concern (VOC) with a high dissemination potential, as it is the case for B.1.617.

Discussion

Sialic acids are used by a wide range of viruses as accessory binding receptors.[22] These glycan groups are found in both glycoproteins and gangliosides of the host cell membrane. However, a clear distinction should be made between sialic acids displayed by glycoprotein and gangliosides, based on their proximity to the cell surface. Gangliosides are flush with the membrane, whereas glycoproteins are more voluminous and thus more distant from the cellular surface. Thus, although glycoprotein sialic acids may facilitate the approach of the virus, only sialic acid bound to gangliosides allow a close contact between the viral envelope and the plasma membrane of target cells. Since gangliosides are concentrated in lipid rafts, these membrane microdomains have a strong electronegative shield that is particularly efficient to concentrate viral particles on the cell surface. Consistently, lipid rafts play a key role in virus infection.[23] In the case of SARS-CoV-2, each subunit of the trimeric spike protein displays two separate domains involved in virus adhesion to the cell surface of host cells. Initially, the RBDs of the three subunits are clustered in the central zone of the spike, whereas the three NTDs are peripheral (Fig. 1). Binding of the NTD to gangliosides is likely to trigger a lipid-dependent, chaperone-like[24] conformational change in the RBD of the neighbor subunit,[25] as shown for the NTD of chain A and the RBD of chain C in Fig. 1. During this process, which is fully conserved among coronaviruses, the RBD undergoes a hinge-like transition from the closed state, moving from a receptor inaccessible to a receptor-accessible topology (open state).[26–28] Similar interfacial/allosteric mechanisms have also been described for other enveloped viruses such as HIV-1.[29]

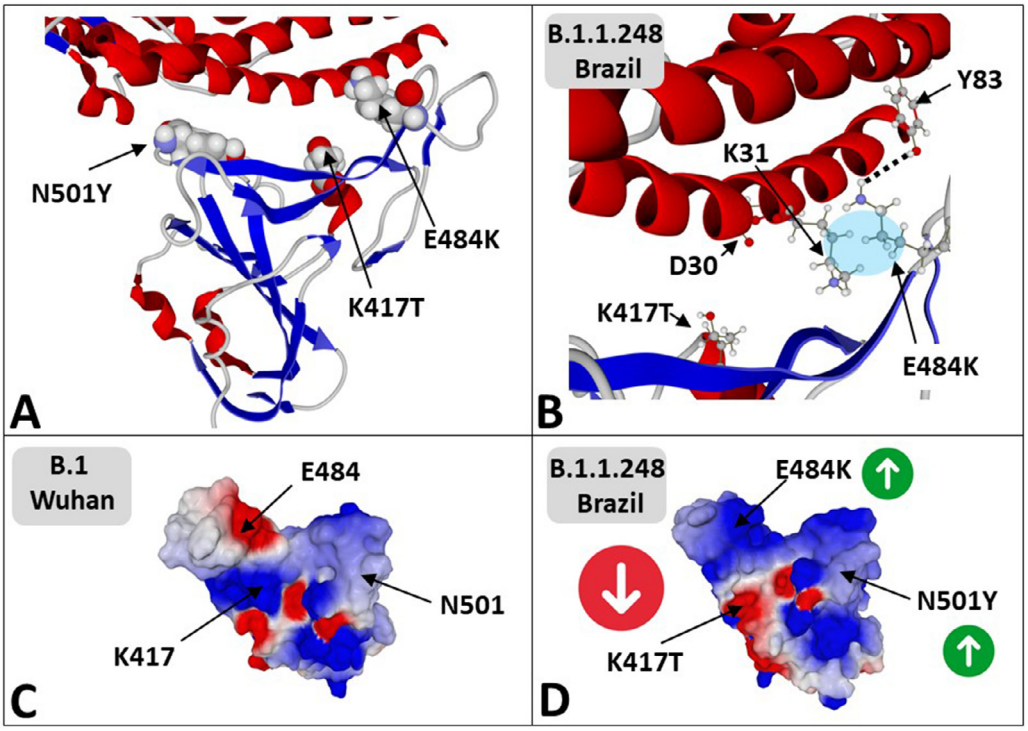

Fig. 7. Impact of mutations K417T, E484K and N501Y (Brazil B.1.1.248 variant) on ACE-2 recognition. A. Overall view of the molecular complex between ACE-2 and the Brazil B.1.1.248 RBD with the three mutations K417T, E484K and N501Y. Both lysine-484 and tyrosine-501 interact closely with ACE-2, whereas threonine-417 has no contact with the receptor. **B.** The side chain of lysine-484 establishes stabilizing van der Waals interactions with methylene groups of lysine-31 (cyan disk) and a hydrogen bond with tyrosine-83 of ACE-2. **C.** Electrostatic surface potential of the Wuhan B.1 RBD with positions 417, 484 and 501 indicated. **D.** Electrostatic surface potential of the Brazil B.1.1.248 RBD (mutations 417, 484 and 501 are indicated). K417T is associated with a loss of positive charge which results in decreased interaction of the RBD with ACE-2. N501Y, which slightly increases the local surface potential, also increases ACE-2 binding. Finally, E484K induces an inversion of the surface potential, which improves ACE-2 recognition.

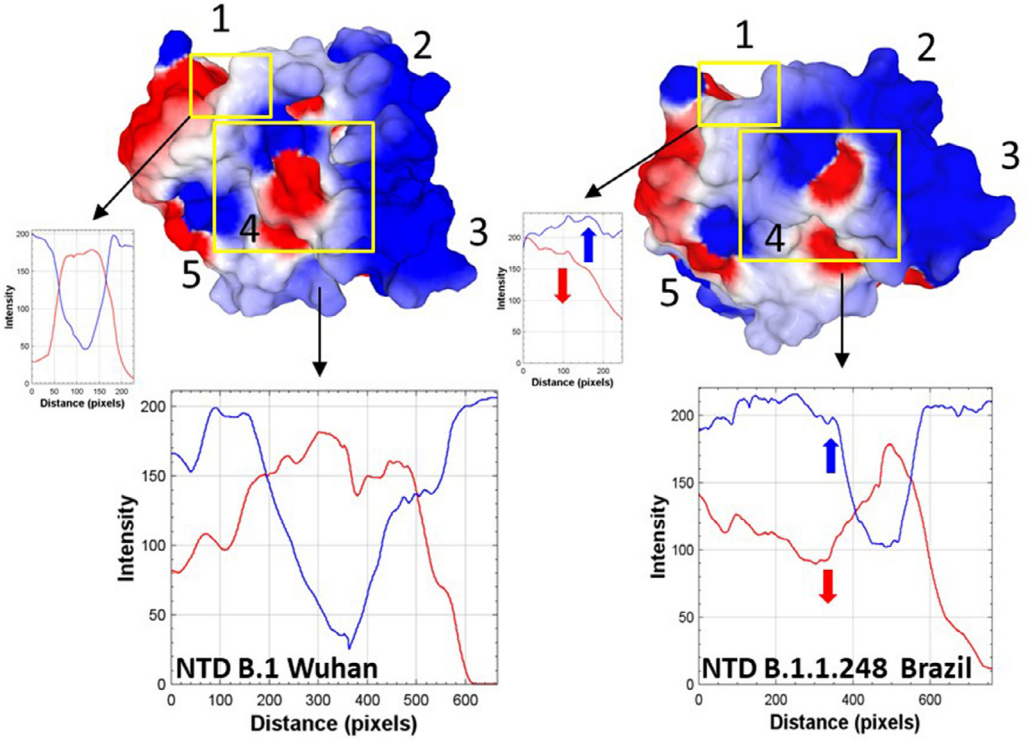

Fig. 8. Impact of mutations L18F, T20N, P26S, D138Y, and R190S on the NTD (Brazil B.1.1.248 variant). The electrostatic surface potential of the Brazil B.1.1.248 NTD shows important changes in charge distribution compared with the Wuhan B.1 NTD. Changes in electrostatic potential affect five distinct zones numbered from 1 to 5. The relative intensity of blue and red colors in regions 1 and 4 (yellow frames) is indicated in the histograms. (For interpretation of the references to colour in this figure legend, the reader is referred to the web version of this article.)

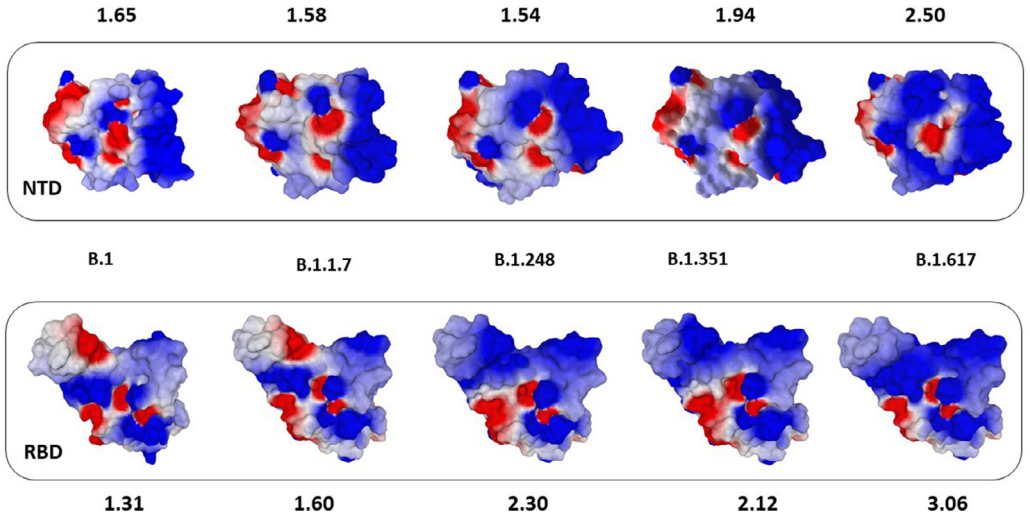

Fig. 9. Comparative analysis of the NTD and RBD surface potential in SARSCoV-2 variants. This analysis illustrates the evolution of the surface potential in both the NTD and the RBD of current circulating SARS-CoV-2 strains over the world. There is a clear tendency to decrease electronegative spots and increase electropositive surfaces. The surface potential values (positive/negative) are indicated (see legend of Table 2 for further details).

Table 2
An index of SARS-CoV-2 transmissibility (T-index) based on kinetics and affinity parameters combining the NTD, the RBD, lipid raft gangliosides and ACE-2.

Virus strain	NTD-ganglioside[1] $\Delta G_{mut}/\Delta G_{wt}$	RBD-ACE-2[2] $\Delta G_{mut}/\Delta G_{wt}$	Surface Potential NTD[3]	Surface Potential RBD[3]	T-index[4]
Wuhan B.1	1	1	1.65	1.31	2.16
UK B.1.1.7	0.98	1.45	1.58	1.60	3.59
Brazil B.1.1.248	1.01	1.02	1.54	2.30	3.65
South Africa B.1.351	0.96	0.97	1.94	2.12	3.82
India B.1.617	1.01	1.38	2.50	3.06	10.67

[1] Calculated from molecular models of NTD bound to lipid raft containing 6 GM1 molecules.
[2] Calculated from molecular models of RBD bound to ACE-2.
[3] Ratio of electropositive (blue) divided by electronegative (red) surfaces of the NTD or the RBD facing the host cell membrane. A value of 1 indicates an electroneutral surface, >1 excess of electropositive charges, <1 excess of electronegative charges.
[4] Transmissibility index (T-index): T-index = $\Delta G_{mut}/\Delta G_{wt\ [NTD\text{-}ganglioside]}$ x $\Delta G_{mut}/\Delta G_{wt\ [RBD\text{-}ACE\text{-}2]}$ x $[\text{Surface Potential}]_{NTD}$ x $[\text{Surface Potential}]_{RBD}$.

The coalescence of a raft bringing ACE-2 with the raft onto which the NTD is bound (Fig. 1) engages the viral particle into an irreversible thermodynamic process which leads to virus fusion or internalization. Disrupting lipid raft organization (e.g. with methyl-β-cyclodextrin treatment) blocks virus infection at this early stage as demonstrated for a broad range of animal and human viruses,[30–32] including coronaviruses in general[33,34] and SARS-CoV-2 in particular.[35] Since lipid raft gangliosides are negatively charged, the electrostatic potential of the spike protein is a key parameter which has to be considered to understand the biology and evolution of SARS-CoV-2 variants.

In this study, we present a new strategy for analyzing the impact of RBD and NTD mutations on the spreading of SARS-CoV-2 variants. The variants studied displayed mutations in both the RBD and the NTD. Indeed, any analysis of the infectivity of such variants should not focus exclusively on the RBD.

Instead, a rational approach is to consider all mutations in these domains that are likely to control the binding of the viral particle to the host cell surface. Given that the virus is attracted to lipid rafts before having a chance to meet ACE-2, it is clear that the electrostatic component of the binding reaction is, at least in the beginning of the adhesion process, especially critical. Thus, it is of primary importance to evaluate the impact of any mutation on the surface potential of both the NTD and the RBD. A virus with an electropositive gain, which, for instance, is conferred by an E→K substitution such as the E484K mutation, will have a kinetic advantage compared with wild-type isolates. The variations in the affinity of the RBD for ACE-2 are significant but moderate. Indeed, increases by 1.5/2-fold are generally considered significant.[36] Under this situation, the kinetic component of the binding reaction driven by the NTD may be preponderant because two viruses that differ only slightly in their affinity for ACE-2 may be selected by the host on the basis of their speed to reach the plasma membrane. Mutations that either decrease electronegativity (e.g. D →Y) or increase electropositivity (e.g. E →K) will give a decisive kinetic advantage for the viruses, with improved access to lipid rafts. It is the case for the UK (B.1.1.7), Brazil (B.1.1.248), South Africa (B.1.351) and India (B.1.617) variants which harbor mutations that induce a dramatic effect on the global surface potential, resulting in faster lipid raft attraction. Moreover, these variants could be classified according to their increase in surface electropositivity (Fig. 9), which could thus serve as a scale for predicting their relative transmissibility.

In this respect, it is worthy to note a striking similarity between virus evolution[37] and protein engineering[38] which are both based on biologically driven (or inspired) changes in the electrostatic surface potential. The tropism evolution of HIV in an infected individual is associated with a switch in co-receptor usage, starting from the slightly electronegative CCR5 to the highly acidic CXCR4.[39] The latter is recognized by HIV strains after several key amino acid changes in the V3 domain of the surface envelope glycoprotein gp120. These changes are chiefly a gradual enrichment in basic amino acid residues (lysine and arginine) which confer a strongly positive surface potential.[40] Highly cationic V3 loops have thus a higher affinity for CXCR4 compared with initial virus isolates.[39] Changes in the surface potential are also believed to play a critical role in the animal to human transmission of several viruses, including influenza.[37] In particular, mutations increasing the charge of the RBD region, which modulate binding avidity and affinity of

influenza hemagglutinin for host receptors, are selected upon antiviral treatment with oseltamivir.[41] Thus, the acquisition of oseltamivir resistance may have contributed to the widespread of influenza virus strains with higher electropositive surface potential.[41] The possibility that such changes could have facilitated the SARS-CoV-2 transfer from human to minks (and potentially back to human)[42] deserves to be investigated. More generally, if we consider the Red Queen aphorism of evolution according to which species run faster and faster to stay at the same place, one could give a response to the question: where do you run – I run to be more positive. In the case of viruses, this trick may not only represent a kinetic advantage for cell surface binding (adaptive selection), but also, in a second step for immune escape.[43] In this respect, one should note the intriguing notion that "fast" viruses selected for their avidity for lipid rafts are, in essence, "pre-selected" to escape immune surveillance (either natural or vaccine-induced) just because their mutation pattern always affects the electrostatic surface potential of neutralizing epitopes. This situation explains why the immune system of HIV-infected patients generally loses the race, the V3 loop running faster and being always too electropositive for neutralizing antibodies. Such a problem could also occur for SARS-CoV-2 vaccines,[44] especially for neutralizing antibodies directed against the NTD which displays a rich panel of mutations compared to the limited number of hot spots in the RBD. For instance the four variants analyzed in the present study has only 4 mutational sites in the RBD (K417, L452, E484, N501) but as much as 3 types of deletions (from 1 to 3 amino acid residues) and 9 mutation spots in the NTD (Table 1). In both cases, most of these mutations have a direct effect of the surface potential. Despite this high level of variability, the energy of interaction of the NTD with raft gangliosides remains mostly unchanged compared to the Wuhan B.1 NTD (Table 2). These observations further support the notion that SARS-CoV-2 evolution is chiefly driven by kinetics rather than affinity parameters inasmuch as initial binding of the virus to host cells is concerned.

Finally, mutations outside the NTD and the RBD, although not directly affecting the binding of SARS-CoV-2 to host cells, may facilitate later steps such as virus fusion through relaxing conformational effects (e.g. D614G) or proteolytic cleavage (P681R).[45] It is interesting to note that for the first six months after the beginning of the pandemic, when most patients did not receive any drug treatment nor vaccine, only the D614G mutation was selected in the spike protein.[46,47] Indeed, mutations in the RBD and in the NTD appeared later, when passive immunotherapy,[48,49] antiviral treatment[50] and then vaccination[51] became widely used. Retrospective studies will help to clarify whereas these strategies might have favored the emergence or perhaps even selected currently circulating variants.

Genomic surveillance is critical for identifying functionally significant variants of SARS-CoV-2 over the world. We propose a new approach to predict, in real time, the spreading capacity of SARS-CoV-2 variants of interest (VOI) as soon as they are detected anywhere in the world. Our strategy is based on a calibrated *in silico* analysis of both the RBD and the NTD in four distinct steps: (i) determination of the electrical surface potential of the NTD, (ii) determination of the electrical surface potential of the RBD, (iii) measurement of the affinity of the RBD for ACE-2, and (iv) evaluation of the avidity of the NTD for lipid raft gangliosides. This analysis has been designed to assess whether the mutations confer a better avidity/affinity for cell surface components (lipid rafts and ACE-2) and/or a faster access to these components through an increase of electropositivity. Combined in a quantitative index (T-index), these 4 parameters may allow a reliable assessment of the transmissibility of emerging variants, which is crucial to timely response of healthcare systems. Variants such as the India B.1.617 with a high T-index are also likely to escape natural or vaccine-induced immunity. We are confident that this new look will give invaluable information for setting a health monitoring of SARS-CoV-2 variants, and identify which variants of interest (VOI) may become variants of concern (VOC). We anticipate that our approach will also be useful for assessing the transmissibility of other viruses such as influenza.

Transparency declaration

Funding

No external funding was received.

Access to data

Not concerned.

Contribution

All authors contributed equally to this study, analyzed the data and wrote the manuscript. J.F. and F.A., molecular modeling; N.Y., sequence data analysis; H.C. molecular analysis of protein-protein complexes.

Declaration of Competing Interest

The authors declare no conflict of interest.

Acknowledgments

We thank Coralie Di Scala for helpful discussions and critical advice.

References

1. Faria NR, Mellan TA, Whittaker C, Claro IM, Candido DDS, Mishra S, Crispim MAE, et al. Genomics and epidemiology of the P.1 SARS-CoV-2 lineage in Manaus, Brazil. *Science* 2021;**372**:815–21.
2. Volz E, Mishra S, Chand M, Barrett JC, Johnson R, Geidelberg L, Hinsley WR, et al. Assessing transmissibility of SARS-CoV-2 lineage B.1.1.7 in England. *Nature* 2021;**593**:266–9.
3. Tegally H, Wilkinson E, Giovanetti M, Iranzadeh A, Fonseca V, Giandhari J, Doolabh D, Pillay S, San EJ, Msomi N, et al. Detection of a SARS-CoV-2 variant of concern in South Africa. *Nature* 2021;**592**:438–43.
4. Vaidyanathan G. Coronavirus variants are spreading in India - what scientists know so far. *Nature* 2021;**593**:321–2.
5. Fantini J, Chahinian H, Yahi N. Leveraging coronavirus binding to gangliosides for innovative vaccine and therapeutic strategies against COVID-19. *Biochem Biophys Res Commun* 2021;**538**:132–6.
6. Shang J, Ye G, Shi K, Wan Y, Luo C, Aihara H, Geng Q, Auerbach A, Li F. Structural basis of receptor recognition by SARS-CoV-2. *Nature* 2020;**581**:221–4.
7. Seyran M, Takayama K, Uversky VN, Lundstrom K, Palù G, Sherchan SP, Attrish D, Rezaei N, Aljabali AAA, Ghosh S, et al. The structural basis of accelerated host cell entry by SARS-CoV-2†. *Febs j* 2020.
8. Hammache D, Yahi N, Piéroni G, Ariasi F, Tamalet C, Fantini J. Sequential interaction of CD4 and HIV-1 gp120 with a reconstituted membrane patch of ganglioside GM3: implications for the role of glycolipids as potential HIV-1 fusion cofactors. *Biochem Biophys Res Commun* 1998;**246**:117–22.
9. Hammache D, Yahi N, Maresca M, Piéroni G, Fantini J. Human erythrocyte glycosphingolipids as alternative cofactors for human immunodeficiency virus type 1 (HIV-1) entry: evidence for CD4-induced interactions between HIV-1 gp120 and reconstituted membrane microdomains of glycosphingolipids (Gb3 and GM3). *J Virol* 1999;**73**:5244–8.
10. Cook GM. Glycobiology of the cell surface: its debt to cell electrophoresis 1940-65. *Electrophoresis* 2016;**37**:1399–406.
11. Sriwilaijaroen N, Suzuki Y. Sialoglycovirology of lectins: sialyl glycan binding of enveloped and non-enveloped viruses. *Methods Mol Biol* 2020;**2132**:483–545.
12. Jacobs AA, van den Berg PA, Bak HJ, de Graaf FK. Localization of lysine residues in the binding domain of the K99 fibrillar subunit of enterotoxigenic Escherichia coli. *Biochim Biophys Acta* 1986;**872**:92–7.
13. Seiradake E, Henaff D, Wodrich H, Billet O, Perreau M, Hippert C, Mennechet F, Schoehn G, Lortat-Jacob H, Dreja H, et al. The cell adhesion molecule "CAR" and sialic acid on human erythrocytes influence adenovirus *in vivo* biodistribution. *PLoS Pathog* 2009;**5**:e1000277.
14. Di Scala C, Fantini J. Hybrid *in silico/in vitro* approaches for the identification of functional cholesterol-binding domains in membrane proteins. *Methods Mol Biol* 2017;**1583**:7–19.

15. Di Scala C, Fantini J, Yahi N, Barrantes FJ, Chahinian H. Anandamide revisited: how cholesterol and ceramides control receptor-dependent and receptor-independent signal transmission pathways of a lipid neurotransmitter. *Biomolecules* 2018;**8**.
16. Jo S, Kim T, Iyer VG, Im W. CHARMM-GUI: a web-based graphical user interface for CHARMM. *J Comput Chem* 2008;**29**:1859–65.
17. Lan J, Ge J, Yu J, Shan S, Zhou H, Fan S, Zhang Q, Shi X, Wang Q, Zhang L, Wang X. Structure of the SARS-CoV-2 spike receptor-binding domain bound to the ACE2 receptor. *Nature* 2020;**581**:215–20.
18. Xu C, Wang Y, Liu C, Zhang C, Han W, Hong X, Wang Y, Hong Q, Wang S, Zhao Q, et al. Conformational dynamics of SARS-CoV-2 trimeric spike glycoprotein in complex with receptor ACE2 revealed by cryo-EM. *Sci Adv* 2021;**7**:eabe5575.
19. Cerutti G, Guo Y, Zhou T, Gorman J, Lee M, Rapp M, Reddem ER, et al. Potent SARS-CoV-2 neutralizing antibodies directed against spike N-terminal domain target a single supersite. *Cell Host Microbe* 2021;**29**:819–33.
20. Fantini J, Di Scala C, Chahinian H, Yahi N. Structural and molecular modelling studies reveal a new mechanism of action of chloroquine and hydroxychloroquine against SARS-CoV-2 infection. *Int J Antimicrob Agents* 2020;**55**:105960.
21. Fantini J, Chahinian H, Yahi N. Synergistic antiviral effect of hydroxychloroquine and azithromycin in combination against SARS-CoV-2: what molecular dynamics studies of virus-host interactions reveal. *Int J Antimicrob Agents* 2020;**56**:106020.
22. Matrosovich M, Herrler G, Klenk HD. Sialic Acid Receptors of Viruses. *Top Curr Chem* 2015;**367**:1–28.
23. Chazal N, Gerlier D. Virus entry, assembly, budding, and membrane rafts. *Microbiol Mol Biol Rev* 2003;**67**:226–37 table of contents.
24. Fantini J, Yahi N. Molecular insights into amyloid regulation by membrane cholesterol and sphingolipids: common mechanisms in neurodegenerative diseases. *Expert Rev Mol Med* 2010;**12**:e27.
25. Wrapp D, Wang N, Corbett KS, Goldsmith JA, Hsieh CL, Abiona O, Graham BS, McLellan JS. Cryo-EM structure of the 2019-nCoV spike in the prefusion conformation. *Science* 2020;**367**:1260–3.
26. Gui M, Song W, Zhou H, Xu J, Chen S, Xiang Y, Wang X. Cryo-electron microscopy structures of the SARS-CoV spike glycoprotein reveal a prerequisite conformational state for receptor binding. *Cell Res* 2017;**27**:119–29.
27. Pallesen J, Wang N, Corbett KS, Wrapp D, Kirchdoerfer RN, Turner HL, Cottrell CA, et al. Immunogenicity and structures of a rationally designed prefusion MERS-CoV spike antigen. *Proc Natl Acad Sci U S A* 2017;**114**:E7348–57.
28. Yuan Y, Cao D, Zhang Y, Ma J, Qi J, Wang Q, Lu G, Wu Y, Yan J, Shi Y, et al. Cryo-EM structures of MERS-CoV and SARS-CoV spike glycoproteins reveal the dynamic receptor binding domains. *Nat Commun* 2017;**8**:15092.
29. Ozorowski G, Pallesen J, de Val N, Lyumkis D, Cottrell CA, Torres JL, Copps J, Stanfield RL, Cupo A, Pugach P, et al. Open and closed structures reveal allostery and pliability in the HIV-1 envelope spike. *Nature* 2017;**547**:360–3.
30. Verma DK, Gupta D, Lal SK. Host lipid rafts play a major role in binding and endocytosis of influenza A virus. *Viruses* 2018;**10**:650.
31. Liao Z, Cimakasky LM, Hampton R, Nguyen DH, Hildreth JE. Lipid rafts and HIV pathogenesis: host membrane cholesterol is required for infection by HIV type 1. *AIDS Res Hum Retroviruses* 2001;**17**:1009–19.
32. Wang Y, Zhang Y, Zhang C, Hu M, Yan Q, Zhao H, Zhang X, Wu Y. Cholesterol-rich lipid rafts in the cellular membrane play an essential role in avian reovirus replication. *Front Microbiol* 2020;**11**:597794.
33. Choi KS, Aizaki H, Lai MM. Murine coronavirus requires lipid rafts for virus entry and cell-cell fusion but not for virus release. *J Virol* 2005;**79**:9862–71.
34. Glende J, Schwegmann-Wessels C, Al-Falah M, Pfefferle S, Qu X, Deng H, et al. Importance of cholesterol-rich membrane microdomains in the interaction of the S protein of SARS-coronavirus with the cellular receptor angiotensin-converting enzyme 2. *Virology* 2008;**381**:215–21.
35. Sofiane F, Lamia T, Mohamed S, Mokrane IO. The Use of cyclodextrin or its complexes as a potential treatment against the 2019 novel coronavirus. A mini-review. *Curr Drug Deliv* 2020;**18**:382–6.
36. Starr TN, Greaney AJ, Hilton SK, Ellis D, Crawford KHD, Dingens AS, Navarro MJ, et al. Deep mutational scanning of SARS-CoV-2 receptor binding domain reveals constraints on folding and ACE2 binding. *Cell* 2020;**182**:1295–310 e1220.
37. Heidari A, Righetto I, Filippini F. Electrostatic variation of haemagglutinin as a hallmark of the evolution of avian influenza viruses. *Sci Rep* 2018;**8**:1929.
38. Buettner K, Kreisig T, Sträter N, Zuchner T. Protein surface charge of trypsinogen changes its activation pattern. *BMC Biotechnol* 2014;**14**:109.
39. Kalinina OV, Pfeifer N, Lengauer T. Modelling binding between CCR5 and CXCR4 receptors and their ligands suggests the surface electrostatic potential of the co-receptor to be a key player in the HIV-1 tropism. *Retrovirology* 2013;**10**:130.
40. Cilliers T, Nhlapo J, Coetzer M, Orlovic D, Ketas T, Olson WC, Moore JP, Trkola A, Morris L. The CCR5 and CXCR4 coreceptors are both used by human immunodeficiency virus type 1 primary isolates from subtype C. *J Virol* 2003;**77**:4449–56.
41. Kobayashi Y, Suzuki Y. Compensatory evolution of net-charge in influenza A virus hemagglutinin. *PLoS ONE* 2012;**7**:e40422.
42. Oude Munnink BB, Sikkema RS, Nieuwenhuijse DF, Molenaar RJ, Munger E, Molenkamp R, van der Spek A, et al. Transmission of SARS-CoV-2 on mink farms between humans and mink and back to humans. *Science* 2021;**371**:172–7.
43. Strelkowa N, Lässig M. Clonal interference in the evolution of influenza. *Genetics* 2012;**192**:671–82.
44. Garcia-Beltran WF, Lam EC, St Denis K, Nitido AD, Garcia ZH, Hauser BM, Feldman J, et al. Multiple SARS-CoV-2 variants escape neutralization by vaccine-induced humoral immunity. *Cell* 2021;**184**:2372–83 e2379.
45. Cherian S., Potdar V., Jadhav S., Yadav P., Gupta N., Das M., Das S., et al. Convergent evolution of SARS-CoV-2 spike mutations, L452R, E484Q and P681R, in the second wave of COVID-19 in Maharashtra, India. bioRxiv 2021:2021.2004.2022.440932.
46. Daniloski Z, Jordan TX, Ilmain JK, Guo X, Bhabha G, tenOever BR, Sanjana NE. The Spike D614G mutation increases SARS-CoV-2 infection of multiple human cell types. *Elife* 2021;**10**:e65365.
47. Peacock TP, Penrice-Randal R, Hiscox JA, Barclay WS. SARS-CoV-2 one year on: evidence for ongoing viral adaptation. *J Gen Virol* 2021;**102**. doi:10.1099/jgv.0.001584.
48. Fierabracci A, Arena A, Rossi P. COVID-19: a review on diagnosis, treatment, and prophylaxis. *Int J Mol Sci* 2020;**21**:5145.
49. Kemp SA, Collier DA, Datir RP, Ferreira I, Gayed S, Jahun A, et al. SARS-CoV-2 evolution during treatment of chronic infection. *Nature* 2021;**592**:277–82.
50. Choi B, Choudhary MC, Regan J, Sparks JA, Padera RF, Qiu X, Solomon IH, Kuo HH, Boucau J, Bowman K, et al. Persistence and evolution of SARS-CoV-2 in an Immunocompromised host. *N Engl J Med* 2020;**383**:2291–3.
51. Zhou D, Dejnirattisai W, Supasa P, Liu C, Mentzer AJ, Ginn HM, et al. Evidence of escape of SARS-CoV-2 variant B.1.351 from natural and vaccine-induced sera. *Cell* 2021;**184**:2348–61 e2346.